PHYSICAL REVIEW D **96,** 053001 (2017)

Discovery probability of next-generation neutrinoless double-β decay experiments

Matteo Agostini[*]
Gran Sasso Science Institute, 67100 L'Aquila, Italy

Giovanni Benato[†]
Department of Physics, University of California, Berkeley, California 94720, USA
and Nuclear Science Division, Lawrence Berkeley National Laboratory, Berkeley, California 74720, USA

Jason A. Detwiler[‡]
Center for Experimental Nuclear Physics and Astrophysics, and Department of Physics,
University of Washington, Seattle, Washington 98115, USA
(Received 8 May 2017; published 7 September 2017)

The Bayesian discovery probability of future experiments searching for neutrinoless double-β decay is evaluated under the popular assumption that neutrinos are their own antiparticles. A Bayesian global fit is performed to construct a probability distribution for the effective Majorana mass, the observable of interest for these experiments. This probability distribution is then combined with the sensitivity of each experiment derived from a heuristic counting analysis. The discovery probability is found to be higher than previously considered, but strongly depends on whether the neutrino mass ordering is normal or inverted. For the inverted ordering, next-generation experiments are likely to observe a signal already during their first operational stages. Even for the normal ordering, in the absence of neutrino mass mechanisms that drive the lightest state or the effective Majorana mass to zero, the probability of discovering neutrinoless double-β decay can reach ∼50% or more in the most promising experiments.

DOI: 10.1103/PhysRevD.96.053001

I. INTRODUCTION

Definitive evidence for nonzero neutrino masses from oscillation experiments has been available for nearly two decades [1–4]. However, the incorporation of neutrino masses into the standard model (SM) of particle physics remains an open issue. Because it is electrically neutral, the neutrino is the only known fundamental fermion that could be its own antiparticle, and obtain its mass through a Majorana mass term [5]. Such a Majorana mass term would violate total lepton number conservation, and naturally emerges in many beyond-the-SM theories [6]. It also emerges in leading theories that explain the dominance of matter over antimatter in the Universe [7], to which we owe our very existence. The motivation to test the Majorana nature of the neutrino has never been higher.

At present, the only feasible method for testing a pure-Majorana SM neutrino without requiring new fields or symmetries is to search for neutrinoless double-β ($0\nu\beta\beta$) decay [8]. In this hypothetical nuclear transition a nucleus of mass number A and charge Z decays as $(A, Z) \rightarrow (A, Z+2) + 2e^-$ [9]. A positive detection would signify the first observation of a matter-creating process (without the balancing emission of antimatter), and would unambiguously establish that neutrinos have a Majorana mass component, independent of the channels involved in the transition or the isotope under study [10,11]. An experimental campaign to search for this process has been underway for decades, and its continuation requires intense effort and significant resources. We set out to explore the justification for such an expenditure, a task for which Bayesian methods are particularly well suited. In this work we present our evaluation, using all available information about neutrino phenomenology, of the Bayesian probability that future $0\nu\beta\beta$ decay searches will prove that neutrinos are Majorana particles.

Neutrino phenomenology is described by an extension of the SM in which three quantum flavor states ν_e, ν_μ, and ν_τ couple to charged leptons via the weak interaction [4]. Such flavor states do not have a fixed mass but are rather a quantum-mechanical superposition of three mass eigenstates ν_1, ν_2, ν_3, with masses m_1, m_2, m_3. The transformation between the mass and flavor bases is described by the unitary Pontecorvo-Maki-Nakagawa-Sakata matrix, which is parametrized by three mixing angles (θ_{12}, θ_{13}, θ_{23}), the CP-violating phase δ, and two Majorana phases (α_{21}, α_{31}). Consequently, neutrinos can transform from one flavor state to another during propagation, giving rise to neutrino oscillation, which remains to date the only observed phenomenon requiring nonzero neutrino masses.

[*]matteo.agostini@gssi.infn.it
[†]gbenato@berkeley.edu
[‡]jasondet@uw.edu

The transformation probability is a function of the two squared mass differences Δm^2_{31} and Δm^2_{21} (where $\Delta m^2_{ij} \equiv m^2_i - m^2_j$), the three mixing angles, and δ. All oscillation parameters have been measured with the exception of δ and the sign of Δm^2_{31} [4,12]. These parameters should be accessible in the near future by experiments exploiting vacuum oscillations or matter-induced flavor transformations [13–16].

Complementary constraints on neutrino phenomenology are provided by cosmological observations, precision measurements of β-decay kinematics, and $0\nu\beta\beta$ decay searches [17,18]. Lepton number violation searches at accelerators and other experimental probes can provide additional information on neutrinos (see, for example, [19,20]) but are not discussed here.

Cosmology is sensitive to the sum of neutrino masses: $\Sigma = m_1 + m_2 + m_3$. The value of Σ is constrained by Planck and other observations [21], which set upper limits on the order of tens to hundreds of meV, depending on the model and data sets used for analysis [22]. A lower limit for Σ is imposed by the measurements of the mass splittings.

The energy spectrum end point of electrons emitted in nuclear β decay is sensitive to the rest mass of the electron antineutrino [23,24]. Since the neutrino mass splittings are smaller than can be resolved with available electron spectroscopic techniques, the end point defect is characterized by the effective neutrino mass

$$m_\beta \equiv \sqrt{m_1^2 c_{12}^2 c_{13}^2 + m_2^2 s_{12}^2 c_{13}^2 + m_3^2 s_{13}^2} \qquad (1)$$

where $s_{ij} = \sin\theta_{ij}$ and $c_{ij} = \cos\theta_{ij}$. A nonzero m_β has not yet been observed and the best upper limits are set by the Troitsk [25] and Mainz [26] experiments, giving $m_\beta < 2.12$ eV at 95% credible interval (CI) and $m_\beta < 2.3$ eV at 95% confidence level (CL), respectively.

The strongest limits on the half life of $0\nu\beta\beta$ decay are from the KamLAND-Zen [27] and GERDA [28] experiments, giving $T_{1/2}(^{136}\mathrm{Xe}) > 10.7 \times 10^{25}$ yr (sensitivity: 5.6×10^{25} yr) and $T_{1/2}(^{76}\mathrm{Ge}) > 5.3 \times 10^{25}$ yr (sensitivity: 4.0×10^{25} yr) at 90% CL, respectively. In a minimal SM extension that incorporates neutrino masses by only adding Majorana neutrino mass terms for the three known mass eigenstates to the SM Lagrangian, $0\nu\beta\beta$ decay is mediated by the exchange of neutrinos. In this case, the half life of the process is given by [29]

$$(T_{1/2})^{-1} = G_{0\nu} |\mathcal{M}_{0\nu}|^2 {m_{\beta\beta}}^2 \qquad (2)$$

where $G_{0\nu}$ is a phase-space factor and $\mathcal{M}_{0\nu}$ is the dimensionless nuclear matrix element (NME) encompassing the nuclear physics. The observable $m_{\beta\beta}$, the effective Majorana mass, is given by

$$m_{\beta\beta} \equiv |m_1 c_{12}^2 c_{13}^2 + m_2 s_{12}^2 c_{13}^2 e^{i\alpha_{21}} + m_3 s_{13}^2 e^{i(\alpha_{31}-\delta)}|. \qquad (3)$$

The aforementioned limits on $T_{1/2}$ translate to $m_{\beta\beta} <$ 61–165 eV and $m_{\beta\beta} <$ 150–330 eV (90% CL) [27,28]. The ranges account for different theoretical calculations of the NME [29].

For light Majorana neutrino exchange, the allowed parameter space for $0\nu\beta\beta$ decay is considerably constrained. In the case $\Delta m^2_{31} < 0$, referred to as the inverted neutrino mass ordering (IO), the oscillation parameters dictate that $m_{\beta\beta}$ cannot be much lower than ~18 meV [16]. A broad international experimental program requiring considerable resources is being mounted to search for $0\nu\beta\beta$ decay in this range. These experiments will also be sensitive to part of the parameter space for the normal ordering (NO, corresponding to $\Delta m^2_{31} > 0$), although if $m_{\beta\beta}$ is exceedingly small even larger experiments will be required.

To maximize the return on this investment, it is the opinion of the authors that the design of these future experiments should be driven by the likelihood of discovering $0\nu\beta\beta$ decay, rather than limit-setting capability as is usually done. With the aim of furthering progress in this direction, this article presents a global Bayesian analysis to extract the present-day probability distribution of $m_{\beta\beta}$ using all relevant experimental information available to date. The probability distribution is folded with the discovery sensitivity of future $0\nu\beta\beta$ decay experiments, computed here with a heuristic counting analysis. As will be seen, the resulting discovery probabilities indicate that next-generation experiments have a high likelihood of observing a signal if neutrinos are indeed Majorana particles.

Our analysis focuses on scenarios in which neither $m_{\beta\beta}$ nor the lightest neutrino mass eigenstate m_l are fixed by mass mechanisms or flavor symmetries that would significantly alter the parameter space of interest [30–32]. To explore the discovery probability of models yielding extreme hierarchical mass spectra (i.e. with $m_l \ll m_2$), [33] we analyze the asymptotic case in which m_l is 0. Projections for models predicting intermediate values of m_l can be obtained by interpolating between our results. We do not consider explicitly scenarios in which $m_{\beta\beta}$ has a fixed value since the posterior distribution would be a trivial delta function and the discovery probability can be directly extracted from the sensitivity of the experiments.

II. GLOBAL FIT

The parameter basis selected for our global fit is $\{\Sigma, \Delta m^2_{21}, \Delta m^2_{31}\,\text{or}\,\Delta m^2_{23}, \theta_{12}, \theta_{13}, \alpha_{21}, (\alpha_{31}-\delta)\}$, where Δm^2_{31} is used for NO and Δm^2_{23} for IO. The notation is taken from Ref [4]. The remaining degrees of freedom of the model

do not affect the analysis and are neglected. Statistical correlations of the parameters in the basis are also negligible [12]. The ignorance on the scale of the parameters is introduced through scale-invariant priors: the priors of the mass observables are logarithmic whereas the priors of angles and phases, whose values are restricted to the range $[0, 2\pi]$, are flat.

The choice of the basis affects our results only slightly as long as the basis covers all degrees of freedom of the problem and its parameters are constrained by the data (see the discussion in Appendix A). Our usage of Σ and the mass splittings to cover the three degrees of freedom related to the neutrino masses is motivated both by physical and statistical arguments. The Δm^2 parameters are direct observables of oscillation experiments and Σ can be physically interpreted as the neutrino mass scale. In addition, Σ is constrained by the data to a finite range and cannot vanish. This is critical for having a normalizable posterior distribution when a scale-invariant prior is employed.

This basis does not accommodate scenarios with extreme hierarchical mass spectra in which m_l is driven to 0. The discovery probability for such hierarchical scenarios can however be easily studied by fixing Σ to its lower limit. It might seem appropriate to use a basis in which Σ is substituted by m_l. This apparently natural choice poses serious difficulties, as the data are not directly sensitive to m_l except in the case of quasidegenerate masses. If used as an element of the basis, its posterior would be strongly influenced by whatever prior is chosen in the low-mass range. The use of scale-invariant priors would then make the $m_{\beta\beta}$ probability distribution non-normalizable without the imposition of an *ad hoc* cutoff on m_l, whose value affects directly the posteriors. The choice of a cutoff could be motivated by theoretical reasons (see e.g. Ref. [34]), but it would still insert into the analysis an arbitrary assumption which affects the results of the fit.

The likelihood function of the available data is constructed as the product of normalized factors, each expressing the conditional probability of a subset of data given the value of an observable,

$$\begin{aligned}\mathcal{L} = {} & \mathcal{L}(\mathcal{D}_{\rm osc}|\Delta m^2_{21}) \cdot \mathcal{L}(\mathcal{D}_{\rm osc}|\Delta m^2_{31}/\Delta m^2_{23}) \\ & \cdot \mathcal{L}(\mathcal{D}_{\rm osc}|s^2_{12}) \cdot \mathcal{L}(\mathcal{D}_{\rm osc}|s^2_{13}) \\ & \cdot \mathcal{L}(\mathcal{D}_{\rm Troitsk}|m_\beta) \cdot \mathcal{L}(\mathcal{D}_{0\nu\beta\beta}|m_{\beta\beta}),\end{aligned} \tag{4}$$

where: $\mathcal{D}_{\rm osc}$ are the oscillation data, whose likelihoods are computed using the NuFIT analysis (v3.0, November 2016) [12]; $\mathcal{D}_{\rm Troitsk}$ refers to the limit from Troitsk [25] (including also the limit from Mainz [26] yields no perceptible change in the $m_{\beta\beta}$ distribution); and $\mathcal{D}_{0\nu\beta\beta}$ is the combined results from GERDA and KamLAND-Zen. The latter is built using the sensitivity of the experiments rather then their actual limits, which are strengthened by background underfluctuations (that is, we consider power-constrained limits [35]). This results in a normalized exponentially decreasing likelihood with 90% quantile at $m_{\beta\beta} = 71$–161 meV, depending on the choice of NME.

The NME values are fixed parameters in this analysis and the impact of their variation is evaluated by performing the calculations multiple times assuming different nuclear models. We consider the quasiparticle random phase approximation (QRPA [36–38]), the interacting shell model (ISM [39,40]), the interacting boson model (IBM-2[41]), and energy density functional theory (EDF [42,43]). Within each model we use the average of the computations performed by different groups, taking the spread as an indication of systematic uncertainty as discussed in Ref. [29]. We perform the primary analysis without considering quenching of the axial vector coupling constant g_A. The effect of variation of g_A is discussed below. For recent insight into the status of the quenching issue we refer the reader to Ref. [29].

The marginalized posterior distributions for all parameters of the basis and observables of interest are computed via Markov-chain Monte Carlo numerical integrations with the BAT toolkit [44]. All marginalized distributions are included in Appendix A. The posterior distributions for $m_{\beta\beta}$ as a function of m_l are shown in Fig. 1, separately for the NO and IO scenarios. The color map indicates the probability density and the solid lines show the maximally allowed parameter space given the constraints on the oscillation parameters from NuFIT. The volume of the allowed parameter space is dominated by the freedom of the Majorana phase values, on which no direct measurement is available. The probability density is clearly nonuniform: high $m_{\beta\beta}$ values are disfavored by the experimental limits on $m_{\beta\beta}$ and m_β; low $m_{\beta\beta}$ values are unlikely because a fine-tuning of the Majorana phases is needed for the right-hand side of Eq. (3) to vanish [45]. m_l is unlikely to assume low values because oscillation experiments constrain Σ to be larger than $|\Delta m^2_{31}|$, and its scale-invariant prior leaves a small volume of probable parameter space near that lower bound over which m_l can become small. Our results are consistent with previous work [45–47] and the differences can be attributed to the different data sets considered.

Figure 2 shows the marginalized posterior distributions for $m_{\beta\beta}$ and the corresponding cumulative distributions. The deformation of the posterior distributions due to the NME is visualized by the band. The 90% probability central interval for $m_{\beta\beta}$ is 20–119 meV assuming IO and 3–104 meV assuming NO, where we have allowed for the maximum variation among the various NME considered. Consequently, the next-generation experiments that aim for a discovery sensitivity of 10–20 meV will cover the true value of $m_{\beta\beta}$ with $> 95\%$ probability assuming IO and with $\sim 50\%$ probability assuming NO. To cover the true value of $m_{\beta\beta}$ in the case of NO with about 90% probability, an experiment should reach a discovery sensitivity of about 5 meV.

Figure 2 shows also the distributions constructed when the data from Planck and other cosmological observations

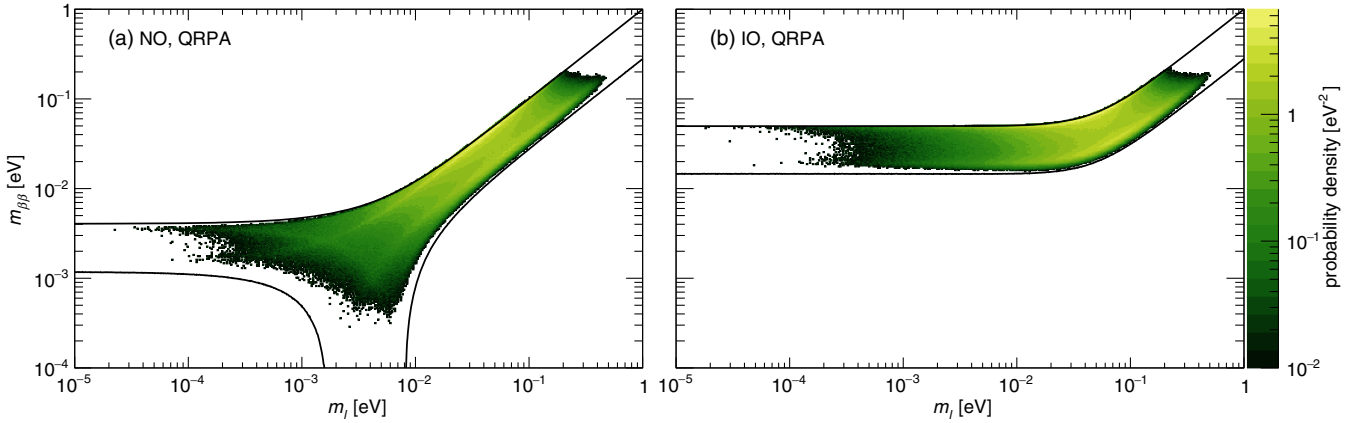

FIG. 1. Marginalized posterior distributions for $m_{\beta\beta}$ and m_l for NO (a) and IO (b). The solid lines show the allowed parameter space assuming 3σ intervals of the neutrino oscillation observables from NuFIT [12]. The plot is produced assuming QRPA NMEs and the absence of mechanisms that drive m_l or $m_{\beta\beta}$ to 0. The probability density is normalized by the logarithm of $m_{\beta\beta}$ and m_l.

are added to the fit as an additional normalized factor of the likelihood $\mathcal{L}(\mathcal{D}_{\rm cosm}|\Sigma)$, where $\mathcal{D}_{\rm cosm}$ represents the observational constraints on Σ from the combination of data labeled as "TT+lowP+lensing+ext" in Ref. [21]. These new data disfavor the quasidegenerate region at high values of m_l and compress the distributions of $m_{\beta\beta}$ to lower values.

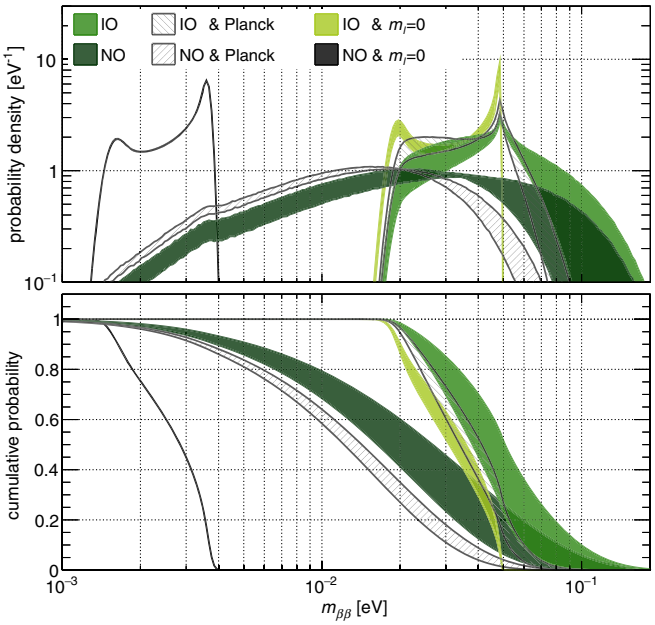

FIG. 2. Top: marginalized posterior distributions of $m_{\beta\beta}$ for NO and IO, normalized by the logarithm of $m_{\beta\beta}$. Bottom: complementary cumulative distribution functions for $m_{\beta\beta}$. The band shows the deformation of the posterior distribution due to different assumptions on the NME. The data from cosmology provide a somewhat stronger constraint on $m_{\beta\beta}$ than the current $0\nu\beta\beta$ decay experiments. The sharp peaks visible in the $m_{\beta\beta}$ distributions are due to a volume effect dominated by Σ and the Majorana phases. For NO with $m_l = 0$ there is negligible variation due to the NME.

In this work, we use as reference results those obtained without imposing cosmological constraints. This choice is motivated by the fact that cosmological constraints are model dependent, not only on the ΛCDM model used to interpret the data, but also on a host of astrophysical models required to extract limits on Σ from disparate data sets with complex and inter-related systematic uncertainties [22,48]. In any case, at present the impact of cosmological data is still limited: the cumulative distributions of $m_{\beta\beta}$, and ultimately also the experimental discovery probabilities, change by only tens of percent.

When the fit is performed with Σ fixed to its minimum allowed value (corresponding to $m_l = 0$), the $m_{\beta\beta}$ posterior distribution is constrained to lie within the horizontal bands that extend to $m_l \to 0$ in Fig. 1. The $m_{\beta\beta}$ posterior distribution is slightly shifted to smaller values for IO, and the discovery probability of future experiments remains very high. In NO, $m_{\beta\beta}$ is pushed below the reach of future experiments, and the discovery probabilities become very small. Using m_l in the fit basis with a log-flat scale-invariant prior would provide the same results as long as the cutoff on m_l, required to have normalizable posterior distributions, is set low enough to make the result independent of the choice of cutoff.

III. EXPERIMENTAL SENSITIVITY

The experimental search for $0\nu\beta\beta$ decay is a very active field. There are a number of isotopes that can undergo $0\nu\beta\beta$ decay and many detection techniques have been developed and tested in recent years [49,50]. Examples are high-purity Ge detectors [51,52], cryogenic bolometers [53,54], loaded organic liquid scintillators [27], time-projection chambers [55,56], and tracking chambers [57]. Various larger-scale experiments with the sensitivity to probe the full IO parameter space are being mounted or proposed for the near or far future. This work focuses on those projects

considered recently by the U.S. DOE/NSF Nuclear Science Advisory Committee's Subcommittee on Neutrinoless Double Beta Decay [58]: CUPID [59,60], KamLAND-Zen [61], LEGEND [62,63], nEXO [64], NEXT [65], PandaX-III [66], SNO+ [67,68], and SuperNEMO [69,70]. Most of these projects follow a staged approach in which the target mass is progressively increased. The various phases and parameters of each project are summarized in Table I and discussed in Appendix C. We caution the reader, however, that many of these experiments are under rapid development, and the parameters publicly available during the snapshot of time in which this manuscript was prepared will often poorly characterize their ultimate reach. Our conclusions should therefore be taken with a heavy grain of salt, and we implore the reader to resist the urge to use our results to make comparisons between experiments, and instead to focus on their combined promise as a global, multi-isotope endeavor. We hope that our methods are also useful as a figure of merit by which individual experiments can evaluate their own implementations. This analysis will be updated as new information becomes available.

A primary experimental signature for $0\nu\beta\beta$ decay is a monoenergetic peak in the measured energy spectrum at the Q value of the decay, produced when the two electrons emitted in the process are fully absorbed in the detector's active volume. While in many detectors additional analysis handles are available to distinguish signal from background, energy is the one observable that is both necessary and sufficient for discovery, and so the sensitivity of a $0\nu\beta\beta$ decay experiment is driven by Poisson statistics for events near the Q value. It can thus be approximated with a heuristic counting analysis, where there are just two parameters of interest: the "sensitive exposure" ($\mathcal{E}$) and the "sensitive background" ($\mathcal{B}$). $\mathcal{E}$ is given by the product of active isotope mass and live time, corrected by the active fiducial volume, the signal detection efficiency, and the probability for a $0\nu\beta\beta$ decay event to fall in the energy region of interest (ROI) in which the experiment is sensitive to the signal. $\mathcal{B}$ is the rate of background events in the ROI after all analysis cuts, with dimensions of counts per unit sensitive exposure. The number of signal and background counts in the final spectrum is then given by

$$N_{0\nu\beta\beta} = \frac{\ln 2 \cdot N_A \cdot \mathcal{E}}{m_a \cdot T_{1/2}} \quad \text{and} \quad N_{bkg} = \mathcal{B} \cdot \mathcal{E} \qquad (5)$$

where N_A is Avogadro's number, m_a is the molar mass of the target isotope, and $T_{1/2}$ is the half-life of the decay.

The experimental efficiencies can be separated into the actual fraction of mass used for analysis ϵ_{FV} (accounting for dead volumes in solid detectors and fiducial volume cuts in liquid and gaseous detectors), the signal efficiency ϵ_{sig} (which is the product of the analysis cut efficiency and the $0\nu\beta\beta$ decay containment efficiency), and the fraction of fully contained $0\nu\beta\beta$ decay events with energy reconstructed in the ROI. The choice of optimal ROI depends on the background rate, its energy distribution, and the energy resolution (σ) of the Gaussian peak expected from the signal. Experiments with excellent energy resolution ($\sigma < 1\%$) have optimal ROIs centered at the Q value with a width depending on the background rate. For experiments with poorer energy resolution, the background due to two-neutrino double-β decay is significant up to the Q value. These experiments have an asymmetric optimal ROI covering primarily the upper half of the Gaussian signal. Our method to compute the optimal ROI is discussed in Appendix B.

With these considerations, the discovery sensitivity for each next-generation experiment is computed using a heuristic counting analysis. In cases where energy spectral fits and position nonuniformity enter nontrivially into the sensitivity (as e.g. in SuperNEMO and nEXO), we tuned our parameters to match the collaboration's stated sensitivity until agreement at the 10%–20% level was achieved. Again, our goal is not to directly compare one experiment to another, but to interpolate the sensitivity curves as a function of live time to allow a study of the discovery probability of the ensemble of proposed experiments. Further details of these computations and the input parameters are discussed in Appendices B and C.

The sensitivity of an experiment to discover a signal is here defined as the value of $T_{1/2}$ or $m_{\beta\beta}$ for which the experiment has a 50% chance to measure a signal with a significance of at least 3σ [71]. Figure 3 plots the $m_{\beta\beta}$ discovery sensitivity as a function of $\mathcal{E}$ and $\mathcal{B}$ for three isotopes. Contours in $m_{\beta\beta}$ are drawn as bands representing the spread in NME for the given isotope. The expected discovery sensitivity of each experiment after 5 years of live time is marked in the plot and also included in Table I. The $T_{1/2}$ sensitivity after 10 years of live time is about a factor $\sqrt{2}$ higher for all experiments considered, although for the lowest background experiments the improvement is as high as a factor of 1.6. For each isotope, next-generation experiments are expected to reach discovery sensitivity over the entire IO parameter space for at least some NME.

IV. DISCOVERY PROBABILITY

The ultimate question that we want to address in this work is the following: what is the probability of detecting a $0\nu\beta\beta$ decay signal assuming that neutrinos are truly Majorana particles? We define this Bayesian discovery probability as the odds of measuring a $0\nu\beta\beta$ decay signal with a significance of at least 3σ. This is computed by folding the discovery sensitivity with the probability distribution of $m_{\beta\beta}$ output by the global fit. Figure 4 shows the evolution of the discovery probability as a function of live time for a selection of next-generation experiments, assuming the absence of mechanisms driving $m_{\beta\beta}$ and

TABLE I. Experimental parameters of next-generation experiments. The quoted mass refers to the $0\nu\beta\beta$ decaying isotope and the energy resolution to the standard deviation (σ). The ROI edges are given in units of σ from the Q-value of the decay. ϵ_{FV} is the fraction of mass used for analysis and ϵ_{sig} is the signal detection efficiency. For SuperNEMO only, the reported ϵ_{sig} encompasses also the fraction of $0\nu\beta\beta$ decay events in the ROI. The sensitive exposure ($\mathcal{E}$) and background ($\mathcal{B}$) are normalized to 1 yr of live time. $\hat{T}_{1/2}$ and $\hat{m}_{\beta\beta}$ are the median 3σ discovery sensitivities assuming 5 years of live time. The $\hat{m}_{\beta\beta}$ ranges account for the different NME calculations considered in the analysis. The last columns show the envisioned reduction of background level and σ, as well as the expected increase of isotope mass, with respect to predecessor experiments which have released data at the time of manuscript preparation; "n/a" indicates that no published experimental data are available yet.

		Iso. mass	σ	ROI	ϵ_{FV}	ϵ_{sig}	$\mathcal{E}$	$\mathcal{B}$	3σ disc. sens.		Required improvement		
Experiment	Iso	[$\mathrm{kg_{iso}}$]	[keV]	[σ]	[%]	[%]	$\left[\frac{\mathrm{kg_{iso}\,yr}}{\mathrm{yr}}\right]$	$\left[\frac{\mathrm{cts}}{\mathrm{kg_{iso}\,ROI\,yr}}\right]$	$\hat{T}_{1/2}$ [yr]	$\hat{m}_{\beta\beta}$ [meV]	Bkg	σ	Iso. mass
LEGEND 200 [62,63]	^{76}Ge	175	1.3	$[-2, 2]$	93	77	119	1.7×10^{-3}	8.4×10^{26}	40–73	3	1	5.7
LEGEND 1k [62,63]	^{76}Ge	873	1.3	$[-2, 2]$	93	77	593	2.8×10^{-4}	4.5×10^{27}	17–31	18	1	29
SuperNEMO [69,70]	^{82}Se	100	51	$[-4, 2]$	100	16	16.5	4.9×10^{-2}	6.1×10^{25}	82–138	49	2	14
CUPID [59,60,72]	^{82}Se	336	2.1	$[-2, 2]$	100	69	221	5.2×10^{-4}	1.8×10^{27}	15–25	n/a	6	n/a
CUORE [53,54]	^{130}Te	206	2.1	$[-1.4, 1.4]$	100	81	141	3.1×10^{-1}	5.4×10^{25}	66–164	6	1	19
CUPID [59,60,72]	^{130}Te	543	2.1	$[-2, 2]$	100	81	422	3.0×10^{-4}	2.1×10^{27}	11–26	3000	1	50
SNO+ Phase I [67,73]	^{130}Te	1357	82	$[-0.5, 1.5]$	20	97	164	8.2×10^{-2}	1.1×10^{26}	46–115	n/a	n/a	n/a
SNO+ Phase II [68]	^{130}Te	7960	57	$[-0.5, 1.5]$	28	97	1326	3.6×10^{-2}	4.8×10^{26}	22–54	n/a	n/a	n/a
KamLAND-Zen 800 [61]	^{136}Xe	750	114	$[0, 1.4]$	64	97	194	3.9×10^{-2}	1.6×10^{26}	47–108	1.5	1	2.1
KamLAND2-Zen [61]	^{136}Xe	1000	60	$[0, 1.4]$	80	97	325	2.1×10^{-3}	8.0×10^{26}	21–49	15	2	2.9
nEXO [74]	^{136}Xe	4507	25	$[-1.2, 1.2]$	60	85	1741	4.4×10^{-4}	4.1×10^{27}	9–22	400	1.2	30
NEXT 100 [65,75]	^{136}Xe	91	7.8	$[-1.3, 2.4]$	88	37	26.5	4.4×10^{-2}	5.3×10^{25}	82–189	n/a	1	20
NEXT 1.5k [76]	^{136}Xe	1367	5.2	$[-1.3, 2.4]$	88	37	398	2.9×10^{-3}	7.9×10^{26}	21–49	n/a	1	300
PandaX-III 200 [66]	^{136}Xe	180	31	$[-2, 2]$	100	35	60.2	4.2×10^{-2}	8.3×10^{25}	65–150	n/a	n/a	n/a
PandaX-III 1k [66]	^{136}Xe	901	10	$[-2, 2]$	100	35	301	1.4×10^{-3}	9.0×10^{26}	20–46	n/a	n/a	n/a

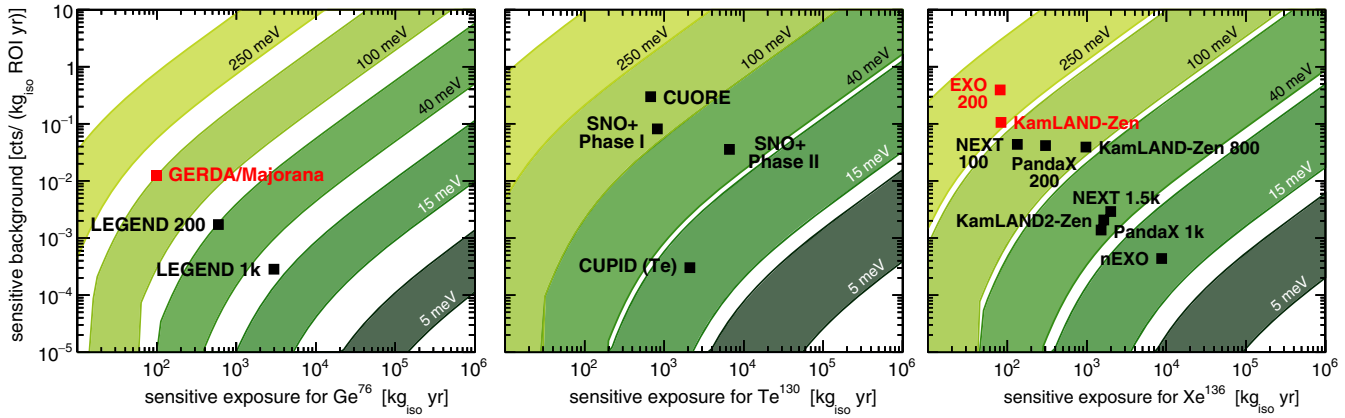

FIG. 3. Discovery sensitivity for ^{76}Ge, ^{130}Te, and ^{136}Xe as a function of sensitive exposure and sensitive background. Contours in $m_{\beta\beta}$ are represented as bands spanning the range of considered NME values. The experimental sensitivities of future or running experiments are marked after 5 years of live time. Past or current experiments with published background level and energy resolution (red marks) are shown according to the average performance in their latest data-taking phase.

m_l to 0. NME variations are visualized as bands. The discovery probability for the most massive experiments exhibits a steep rise already in the first year or two of data taking. And while they begin to flatten after 5 years, each experiment continues to gain discovery probability out to 10 years.

For the case of Majorana neutrinos with an inverted mass ordering, next-generation experiments in each isotope are almost certain to observe a signal in just 5 years of live time. Even several near-term experiments, SNO+ Phase I, KamLAND-Zen 800, and LEGEND 200, have significant chances of discovery before the larger experiments come online. Remarkably, several experiments also reach a discovery probability of over 50% in the case of NO. This strong possibility for discovery in our reference analysis arises from the fact that even though the NO parameter space extends down to exceedingly small $m_{\beta\beta}$, the amount of parameter space left at high $m_{\beta\beta}$ comprises a significant fraction.

One subtlety to note about the bands is that, while their width is driven by the NME variation, the relationship between the discovery probability curves and the NME values is not monotonic. A change in the NME model shifts the discovery sensitivity to higher or lower $m_{\beta\beta}$ for all

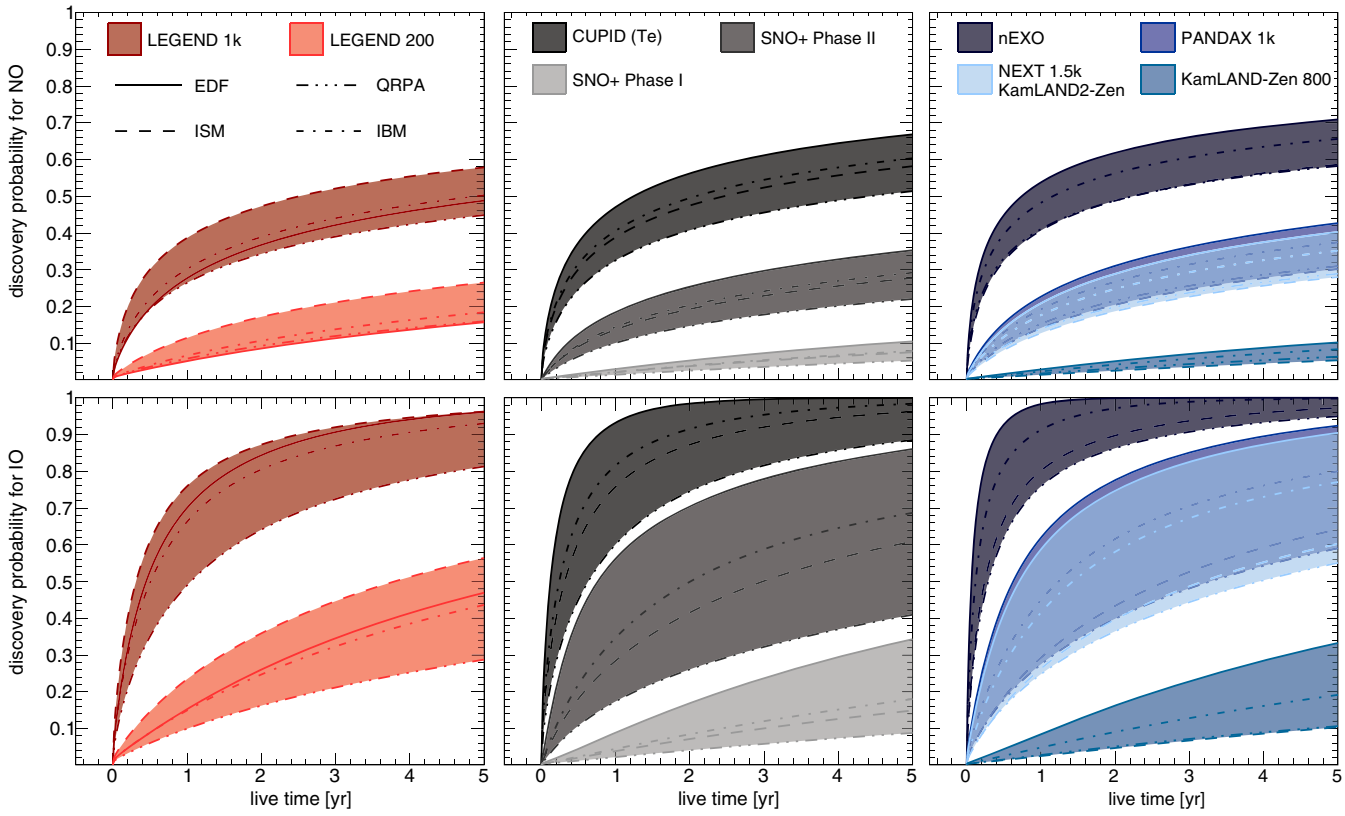

FIG. 4. Discovery probability as a function of live time for a selection of next-generation experiments grouped according to the target isotope (from left to right, ^{76}Ge, ^{130}Te, ^{136}Xe), assuming the absence of mechanisms that drive m_l or $m_{\beta\beta}$ to 0. The top panels show the discovery probability for NO, the bottom panels for IO. The variation of the NME among models is represented by the shaded regions.

isotopes. But the KamLAND-Zen and GERDA constraints result in parameter space opening up or being excluded at high $m_{\beta\beta}$ depending on just the changes in the ^{136}Xe and ^{76}Ge NME values. This leads to both a shift and a subtle distortion of the $m_{\beta\beta}$ probability distribution. The ultimate change in the discovery probability is a nontrivial combination of these shifts and distortions.

We explored the impact on the discovery probabilities of adding also cosmological constraints to our global fit. As expected based on the small deviations that these constraints generate in the $m_{\beta\beta}$ distribution, we find that the discovery probability only degrades by ∼30% for NO. In the case of IO, the discovery probability of future experiments is so strong that cosmological constraints are almost irrelevant.

We also explored the impact of g_A quenching on the discovery probabilities. Quenching degrades the sensitivity of future $0\nu\beta\beta$ decay experiments, making parameter space at low $m_{\beta\beta}$ inaccessible. For a given half-life, the corresponding value of $m_{\beta\beta}$ scales roughly like g_A^{-2}, so that even just ∼30% quenching can degrade an experiment's discovery sensitivity by a factor of 2. However, quenching also relaxes the constraints imposed on $m_{\beta\beta}$ by existing experiments, opening up additional parameter space at high $m_{\beta\beta}$. As a result, the impact on discovery potential is not nearly as large as on the sensitivity. We find that a reduction of g_A by 30% reduces the discovery power by ∼15% (∼25%) for the most promising future experiments in our reference analysis for IO (NO).

When we include both 30% quenching as well as cosmological constraints, the region at high $m_{\beta\beta}$ stays disfavored and the future experiments simply lose reach. In this case we see the biggest suppression in discovery power. However, even in this most pessimistic case the most promising experiments still have discovery power well above 50% in the IO, and in the tens-of-percent range for NO.

The preceding discussion refers to our reference analysis. To explore the case of extreme hierarchical neutrino masses, we repeat the analysis by fixing Σ to its minimum allowed value. We find that for the IO the discovery probability is only marginally impacted for the most promising next-generation experiments, decreasing by at most 10%. For the NO, as expected, the discovery probability drops to 2% or lower for all experiments and for all NME considered.

As a final note, we consider the impact of KATRIN [77], which will perform a tritium-end-point-defect-based kinematic measurement of the effective neutrino mass m_β with 90% CL limit-setting sensitivity of 200 meV, and 5σ discovery level of 350 meV [78]. An upper limit by KATRIN would have a marginal impact: including a 90% CL upper limit on

m_β at 200 meV reduces discovery probabilities negligibly for the IO, and by less than 10% for the NO. A discovery by KATRIN, on the other hand, would be game-changing. Including a KATRIN signal consistent with $m_\beta = 350$ meV in our global analysis results in discovery probabilities in excess of 99% for both IO and NO, for all NME. In this case neutrino masses would be in the quasidegenerate region, and $0\nu\beta\beta$ decay experiments could not distinguish between NO and IO (cf. Fig. 6). Conversely, a nonobservation of neutrinoless double-β decay in that scenario would reject the standard light, left-handed Majorana neutrino exchange mechanism at high confidence level.

V. CONCLUSIONS

The probability distribution for the effective Majorana mass has been extracted with a Bayesian global fit using all experimental information available to date and exploring various assumptions. If the Majorana phases are not fixed by a flavor symmetry and the lightest mass eigenvalue is not driven to 0, this distribution is found to peak at high values of $m_{\beta\beta}$ not far from existing limits. This puts much of the remaining parameter space within the reach of next-generation experiments; it arises from the freedom of the Majorana phases and our requirement that the basis choice yield a normalizable posterior distribution when scale-invariant priors are used.

The sensitivity of a suite of next-generation $0\nu\beta\beta$ decay experiments was estimated with a heuristic counting analysis based on two parameters which fully determine the performance of an experiment: the sensitive background and the sensitive exposure. The sensitivity is finally combined with the probability distribution of the effective Majorana mass to derive the discovery probability.

The discovery probability is found in general to be higher than previously considered for both mass orderings. For the inverted ordering, next-generation experiments are likely to observe a signal already during their first operational stages independent of the considered assumptions. Even for the normal ordering, in the absence of neutrino mass mechanisms that drive the lightest state or the effective Majorana mass to 0, the probability of discovering $0\nu\beta\beta$ decay reaches ~50% or higher in the most promising experiments. These conclusions do not change qualitatively when cosmological constraints are imposed, or when we allow for g_A quenching.

Our results indicate that even if oscillation experiments or cosmological observations begin to strongly indicate a normal ordering (as e.g. in Ref. [79]), next-generation $0\nu\beta\beta$ decay experiments still probe a relevant region of the parameter space and give a valuable return on investment.

ACKNOWLEDGMENTS

The authors thank A. Caldwell, S. R. Elliott, G. Orebi Gann, J. J. Gomez-Cadenas, C. Peña Garay, G. Gratta, Y. Mei, J. Klein, Yu. G. Kolomensky, C. Licciardi, L. Pandola, D. Radford, S. Sangiorgio, B. Schwingenheuer, S. Schönert, F. Vissani, and D. Waters for valuable discussions and suggestions. We are also grateful to the members of the NuFIT project (I. Esteban, C. Gonzalez Garcia, M. Maltoni, I. Martinez Soler, and T. Schwetz) for making their valuable results freely available to the community. M. A. acknowledges support by the Deutsche Forschungsgemeinschaft (SFB No. 1258).

Note added.—On the date of submission of our manuscript, a work by A. Caldwell and others [80] became public on the arXiv. They also perform a Bayesian global analysis of all data to extract a probability distribution for $m_{\beta\beta}$. Although their work has some similarities with ours, the most important difference is their use of the lightest mass eigenvalue (m_l) in the fit basis instead of Σ. When they use a flat prior for m_l, their results are in qualitative agreement with ours, including both discovery probabilities of future experiments as well as the relative impact of cosmological constraints. However, when they use a log-flat prior (with cutoff set to 10^{-7} eV), they find a degraded discovery probability, precisely as we discuss in Sec. II. There are a few other key differences worth highlighting. Caldwell *et al.* extend their Bayesian analysis to include also priors on NME (primarily variations of QRPA) as well as the mass orderings, which we treat independently. They do not consider quenching of the NME. They also use a posterior odds threshold of 99% as the criterion for discovery, as opposed to our choice of 3σ.

APPENDIX A: GLOBAL FIT DETAILS AND STABILITY

The marginalized posterior distributions for all the basis parameters used in the global fit are shown in Fig. 5, along with the posterior distributions for other physical parameters of interest. The bands show the deformation of the distributions due to the NME values.

The posterior distributions of the angles and mass splittings are Gaussian and well defined. The shifts between IO and NO probability distributions come from the results of oscillation experiments [12]. The posterior distributions of the Majorana phases contain some information as the current limits on $0\nu\beta\beta$ decay force a partial cancellation between the three terms on the right-hand side of Eq. (3). The posterior distribution for α_{21} is more informative than for $(\delta - \alpha_{31})$ as the absolute value of the second term is larger than the third one. The distributions of the parameters related to the mass eigenvalues are considerably different for NO and IO as one would expect. The posteriors of the mass eigenvalues and mass observables are constrained to a finite range because of the relative volumes in the likelihood space. For completeness, Fig. 6 shows the correlations between the posterior distributions of the mass observables Σ, $m_{\beta\beta}$ and m_β, obtained assuming QRPA NMEs.

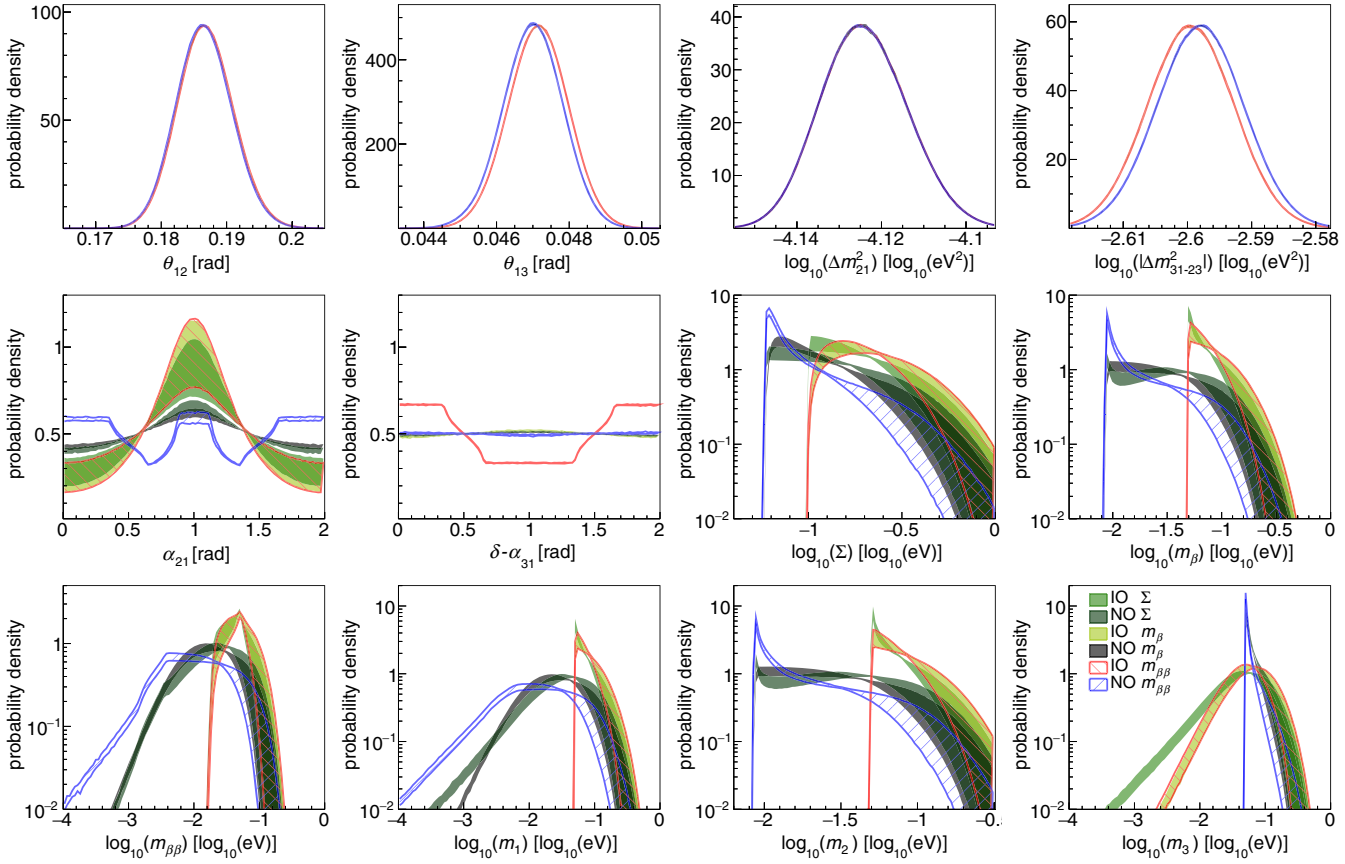

FIG. 5. Marginalized posterior distributions for NO and IO. The band shows the deformation of the posterior distributions due to different assumptions on the NME. For each parameter three bands are displayed, corresponding to different parametrization of the basis in the fit. The lighter bands are obtained with the reference basis; the darker band is obtained for a basis in which Σ is replaced by m_β, and the red and blue bands are obtained by replacing Σ with $m_{\beta\beta}$.

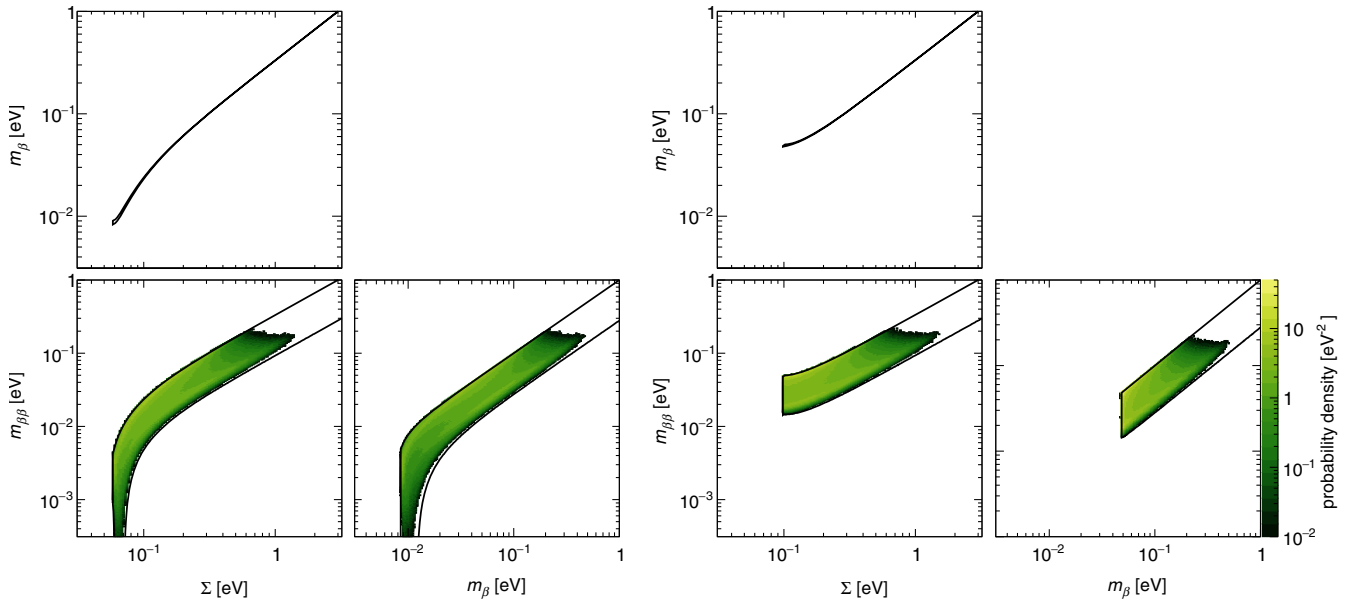

FIG. 6. Marginalized posterior distributions for the mass observables assuming NO (left) and IO (right).The computation is performed assuming QRPA NMEs and the absence of mechanisms that drive m_l or $m_{\beta\beta}$ to 0. The solid lines show the allowed parameter space assuming 3σ intervals of the neutrino oscillation observables from NuFIT [12]. The probability density is normalized by the logarithms of the mass observables.

There are three arbitrary elements in our analysis: the sets of data included in the analysis, the priors, and the parametrization of the model (i.e. the fit basis). The impact of the data set has already been discussed in the extreme case in which Planck results are added to the analysis. This changes the posterior distributions by about 10%–20%.

The impact of the priors is in general weak as the data are strongly informative for most of the parameters in the basis, with the exception of the Majorana phases and Σ. Using a flat prior for Majorana phases seems the only reasonable choice: the parameter ranges are well defined and no information is available on them. The prior used for Σ is logarithmic to preserve scale invariance. An alternative choice would be a flat prior: this would favor larger values of Σ and inflate the discovery probabilities.

The parametrization of the model has potentially a huge impact on the results. For this reason different parametrizations have been tested and the impact on the posterior for $m_{\beta\beta}$ was found to be in general marginal as long as the basis covers all the degrees of freedom of the model and its parameters are constrained by the data. For instance, Fig. 5 shows the posterior distributions obtained when Σ is replaced by m_β in the fit basis (maintaining the logarithmic prior). As occurs for Σ, lower m_β values are prohibited by oscillation experiments and the parameter cannot vanish. The posteriors are basically unchanged with the understandable exception of Σ and m_β.

Conversely, if a parameter of the basis is not sensitive to the data (e.g. low values of m_l) its posterior probability coincides with the prior, and in the case of our log-flat prior the resulting distribution cannot be normalized. When Σ is fixed to its minimum allowed value to study extreme hierarchical models in which $m_l = 0$, the posteriors become trivial: all mass eigenvalues, Σ, and m_β are sharply peaked at their minimum allowed values, while posteriors for square mass differences and angles are nearly indistinguishable from the results of our reference parametrization. Meanwhile, $m_{\beta\beta}$ is pushed to lower values as shown in Fig. 2.

Although there is no deep physical motivation to treat $m_{\beta\beta}$ itself as a fundamental parameter, for completeness we also performed the analysis substituting Σ with $m_{\beta\beta}$ in the parameter basis. For the IO, all posterior distributions except those of the Majorana phases coincide with the posteriors obtained with m_β in the basis. For the NO, $m_{\beta\beta}$ could be vanishingly small, so the results depend, in principle, on the choice of the cutoff as for the case of the basis with m_l. However, with our flat priors for the Majorana phases, values of $m_{\beta\beta}$ below $\sim 10^{-3}$ eV are strongly suppressed and the posterior of $m_{\beta\beta}$ is not affected by the cutoff choice as long as it is $\lesssim 10^{-5}$ eV. The posterior for $m_{\beta\beta}$ shows a preference for lower values with respect to what is obtained with our reference fit, which can be interpreted as a volume effect coming from the assignment of a log-flat prior on $m_{\beta\beta}$ instead of on Σ. Additionally, the posteriors for the Majorana phases show different features with respect to what is obtained with the other bases. Again, these are the results of volume effects and indicate that the current knowledge does not allow us to make any clear statement on the Majorana phases.

APPENDIX B: HEURISTIC COUNTING ANALYSIS

In this work, the discovery sensitivity is defined to be the value of $T_{1/2}$ or $m_{\beta\beta}$ for which an experiment has a 50% chance to measure a signal above background with a significance of at least 3σ. The computation is performed for $T_{1/2}$ and the result is converted to a range of $m_{\beta\beta}$ values using Eq. (2) with different NME values. Given an expectation for the background counts in the ROI of $B = \mathcal{B}\mathcal{E}$, the sensitivity for $T_{1/2}$ is given by

$$T_{1/2} = \ln 2 \frac{N_A \mathcal{E}}{m_a S_{3\sigma}(B)}, \tag{B1}$$

where $S_{3\sigma}(B)$ denotes the Poisson signal expectation at which 50% of the measurements in an ensemble of identical experiments would report a 3σ positive fluctuation above B. If B is large then $S_{3\sigma}(B) \propto \sqrt{B}$, while if $B(t) \ll 1$ then $S_{3\sigma}(B)$ is a constant. To transition smoothly between these two regimes, we find the number of counts $C_{3\sigma}$ such that the cumulative Poisson distribution with mean B satisfies $\mathrm{CDF}_{\mathrm{Poisson}}(C_{3\sigma}|B) = 3\sigma$, and then obtain $S_{3\sigma}$ by solving $\overline{\mathrm{CDF}}_{\mathrm{Poisson}}(C_{3\sigma}|S_{3\sigma} + B) = 50\%$, as suggested in [81] (where $\overline{\mathrm{CDF}}$ refers to the complementary CDF). While $C_{3\sigma}$ should strictly be integer valued, restricting it as such would result in discrete jumps in the discovery sensitivity as B increases. To smooth over these jumps we extend $\mathrm{CDF}_{\mathrm{Poisson}}$ to a continuous distribution in C using its definition via the normalized upper incomplete gamma function,

$$\mathrm{CDF}_{\mathrm{Poisson}}(C|\mu) = \frac{\Gamma(C+1,\mu)}{\Gamma(C+1)}. \tag{B2}$$

Using Eq. (B2), $S_{3\sigma}$ varies smoothly and monotonically with B for values greater than $-\ln[erf(3/\sqrt{2})] = 0.0027$ counts. Below this value of B, the observation of a single count represents a 3σ discovery, marking this as the level at which an experiment becomes effectively "background free" under this metric. In this regime, $S_{3\sigma}$ takes the constant value $\ln 2$.

Using Eqs. (B1) and (B2), the $T_{1/2}$ sensitivity for ^{76}Ge as a function of $\mathcal{E}$ and $\mathcal{B}$ is shown in Fig. 7. Values for other isotopes can be obtained by dividing by the ratio of their molar mass to that of ^{76}Ge. Discovery sensitivity increases linearly with exposure until the experiment exceeds the background-free threshold of 0.0027 counts. For a given exposure, the sensitivity degrades rapidly with background level.

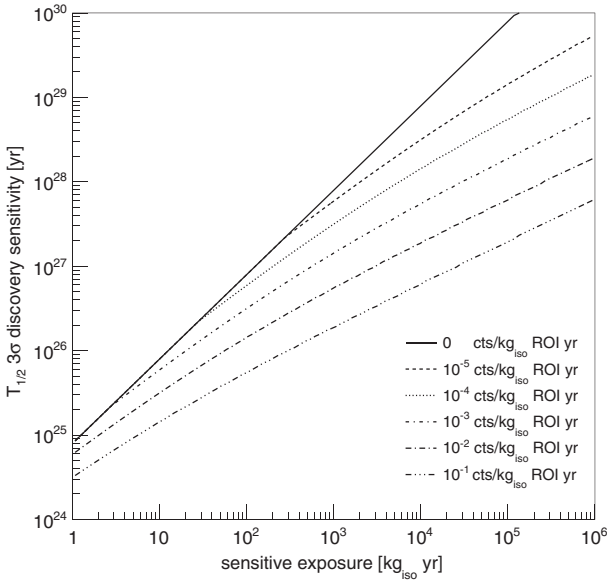

FIG. 7. ^{76}Ge $T_{1/2}$ discovery sensitivity as a function of sensitive exposure for a selection of sensitive background levels.

In a similar manner, the discovery probability is defined to be the probability that an experiment measures a 3σ positive fluctuation above B, given the probability distribution function $dP/dm_{\beta\beta}$ for $m_{\beta\beta}$ (i.e. Fig. 2). Explicitly, the discovery power (DP) is computed as

$$\mathrm{DP} = \int_0^\infty \frac{dP}{dm_{\beta\beta}} \overline{\mathrm{CDF}}_{\mathrm{Poisson}}(C_{3\sigma}|S(m_{\beta\beta}) + B) dm_{\beta\beta}, \quad \text{(B3)}$$

where $S(m_{\beta\beta})$ is the expected signal counts in the experiment for a given value of $m_{\beta\beta}$.

For high resolution experiments with flat background spectra in the vicinity of the Q value, we performed an optimization of the ROI width by maximizing the figure of merit

$$\text{F.O.M.} = \frac{erf(n/\sqrt{2})}{S_{3\sigma}(2bn)} \quad \text{(B4)}$$

where n is the ROI half-width in units of the energy resolution (σ), and b is the background counts per unit σ at 5 years of live time. Since $S_{3\sigma}(2bn) \propto \sqrt{2bn}$ for large values of b, in this regime the figure of merit (F.O.M.) is maximal for the value of n that solves the transcendental equation $ne^{-n^2/2} = erf(n/\sqrt{2})\sqrt{\pi}/4$. This gives an optimal ROI width of 2.8σ for background-dominated experiments, with a corresponding signal efficiency of 84%. At lower background the sensitivity improves with a wider ROI. In the background-free regime, the F.O.M. is optimized when the ROI width is expanded until the region contains 0.0027 counts. Above this region, the F.O.M. was maximized numerically, making use of Eq. (B2). The deviations from the asymptotic value of 2.8 were plotted on a log-log scale and were found to be well approximated by a second-order polynomial. This gives the following expression for the optimum ROI width in units of σ, accurate to $< 1\%$,

$$\mathrm{ROI}_{\mathrm{opt}} = 2.8 + 10^{a_0 + a_1 \log_{10} b + a_2 (\log_{10} b)^2} \quad \text{(B5)}$$

where the parameter values are $a_0 = -0.48$, $a_1 = -0.32$, and $a_2 = -0.046$.

Our treatment ignores uncertainty in the background rate as well as systematic uncertainties. Backgrounds are typically well constrained in $0\nu\beta\beta$ decay experiments using sidebands in energy and, for some detectors, position. Similarly, systematic uncertainties are typically well below 10%. This makes these sources of uncertainty subdominant to the large fluctuations characteristic of low-count-rate Poisson statistics.

APPENDIX C: EXPERIMENTAL PARAMETERS

This appendix discusses the experiments and parameters listed in Table I. The parameter values are taken from official publications and presentations of each collaboration. If not available, the values are assumed to be the same as predecessor or similar experiments (e.g. the instrumental efficiency is usually not given prior to the construction and operation of an experiment). Our heuristic counting analysis is used to derive the sensitivity of each experiment for both a limit-setting and a signal discovery analysis [35]. The collaborations typically quote only the former, but this is enough to cross-check—and possibly tune—the sensitive background and exposure used for this work. Given the values in Table I, our calculation reproduces the official sensitivities quoted by each experiment with 10%–20% accuracy.

LEGEND [62,63] is the successor of GERDA and MAJORANA [51,52]. The project consists of two stages: LEGEND 200 and LEGEND 1k. In the first phase, 200 kg of germanium detectors enriched at 87% in ^{76}Ge will be operated in the existing GERDA infrastructure. The background level measured in GERDA Phase II is $\mathcal{B} = 1.2 \times 10^{-2}$ cts/($\mathrm{kg_{iso}}$ROIyr) on average and 5.1×10^{-3} cts/($\mathrm{kg_{iso}}$ ROI yr) when only the new generation BEGe-type detectors are considered [63]. Compared to the results obtained with BEGe detectors, a further reduction of a factor ~3 is expected in LEGEND 200. For LEGEND 1k, a new infrastructure able to host 1 ton of target mass and a further sixfold background reduction are conceived. We assume the same resolution achieved by the running experiments [~3 keV full width at half maximum (FWHM)], and use a ROI of (Q value $\pm 2\sigma$). Enrichment, active volume, containment and instrumental efficiency are taken from Ref. [28]. Our calculation agrees with the sensitivity

projections of the collaboration [62,63] when the same ROI is used.

SuperNEMO [69,70] is an upgrade of the NEMO-3 experiment. This is the only experiment considered here in which the $0\nu\beta\beta$ decay isotope is separate from the detector. SuperNEMO will consists of 20 identical tracking chambers, each containing ∼5 kg of ^{82}Se embedded in Mylar foils. SuperNEMO can measure independently the energy and direction of the two electrons emitted by $0\nu\beta\beta$ decays, and distinguish different decay channels [70]. The electrons do not release all their energy in the chamber: the expected $0\nu\beta\beta$ decay signature for ^{82}Se is thus a Gaussian peak at ∼2830 keV, about 170 keV below the ^{82}Se Q value [70]. The product of containment and instrumental efficiency for ^{82}Se $0\nu\beta\beta$ decay events is quoted to be 28.2% in Ref. [70]. However, the $0\nu\beta\beta$ decay peak is on the tail of the $2\nu\beta\beta$ decay spectrum (see Fig. 5 of Ref. [70]). We therefore extracted the expected total efficiency and total number of background counts for different energy ranges, and use the ones providing the best sensitivity, i.e. [2800,3100] keV. The corresponding total efficiency, which also includes the fraction of $0\nu\beta\beta$ decay events falling within the ROI, is taken to be 16.5%. With such parameters, we accurately reproduce the official sensitivity [70]. SuperNEMO expects to improve their energy resolution by a factor of 2 and the background level by a factor of ∼50 with respect to NEMO-3 [69,70].

CUPID [59,60,72] is an upgrade of the CUORE experiment [53,54]. In CUORE, ∼1000 TeO_2 crystals with natural isotopic composition are operated as calorimeters (bolometers) at a base temperature of ∼10 mK. CUPID plans to exploit the CUORE cryogenic infrastructure, and increase the sensitivity to $0\nu\beta\beta$ decay using enriched crystals with α/β discrimination capabilities. Several crystals with different double-β decaying isotopes are under investigation, including TeO_2, $ZnMoO_4$, ZnSe and $CdWO_4$. We quote results only for TeO_2 and ZnSe, which we found to yield the lowest background and the highest sensitivity. Both CUORE and CUPID aim at an energy resolution of ∼0.2% (FWHM), which has been proven on a large array of TeO_2 crystals in CUORE-0 [82]. In CUORE, a background level reduction of a factor ∼6 with respect to CUORE-0 is expected thanks to improved shielding and a careful selection of all materials [83]. A further reduction in background level by a factor ∼500 is conceived for CUPID with TeO_2: this can be achieved thanks to the readout of Cherenkov light induced by electrons in TeO_2, or of the scintillation light in the other crystals mentioned above. The optimal ROI for CUORE and CUPID are (Q value $\pm 1.4\sigma$) and (Q value $\pm 2\sigma$), respectively. For both experiments we used an instrumental efficiency of 92% as in its predecessor CUORE-0 [82]. The exclusion sensitivity we obtained differs by $\lesssim$10% from the official values [59,84].

SNO+ is an ongoing upgrade of SNO. It is a multipurpose neutrino experiment, with a $0\nu\beta\beta$ decay search as one of its main physics goals [67,73]. An acrylic sphere with about 800 tons of liquid scintillator, loaded with tellurium, is encompassed by a water buffer. A multistaged approach is foreseen. In SNO+ Phase I, ∼1.3 tons of ^{130}Te are used and an energy resolution of 7.5% FWHM is expected. The goal of SNO+ Phase II [68] is to increase the ^{130}Te mass to ∼8 tons and improve the energy resolution to 5.3%. This is achievable thanks to an improvement of the light yield to 800 pe/MeV [85]. We assumed a containment efficiency of 100% and an instrumental efficiency of ∼97% as for KamLAND-Zen. Using an asymmetric ROI of (Q value $^{+1.5}_{-0.5}\sigma$) [67,68,73], we reproduce the official limit-setting sensitivity [73] with a few percent accuracy.

KamLAND-Zen is a KamLAND upgrade tailored to the search of $0\nu\beta\beta$ decay: a nylon balloon is inserted in the active detector volume and filled with liquid scintillator loaded with enriched xenon. After two successful data-taking phases [27,86], the KamLAND-Zen collaboration is currently preparing two additional phases called KamLAND-Zen 800 and KamLAND2-Zen in which 750 kg and 1 ton of ^{136}Xe will be deployed, respectively. A major upgrade of the experiment is conceived for KamLAND2-Zen to improve the energy resolution at the ^{136}Xe Q values from 4.6% to 2% (σ) and to reduce the background by an order of magnitude. The upgrade includes the installation of new light concentrators and photomultiplier tubes with higher quantum efficiency [61] as well as purer liquid scintillator. In our study we used the same instrumental efficiency as reported in Ref. [27]. The optimal ROI is asymmetric, covering only the upper half of the expected $0\nu\beta\beta$ decay peak to avoid the background due to the $2\nu\beta\beta$ decay spectrum tail. Our calculations reproduce the sensitivities presented in [27,61,86] within 20%. The background measured in KamLAND-Zen phase 2 is $\mathcal{B} = 1.1 \times 10^{-1}$ cts/(kg$_{\rm iso}$ ROI yr) on average, and 5.9×10^{-2} cts/(kg$_{\rm iso}$ ROI yr) when only the second part of the data taking is considered (period 2). Compared to this last result, a further reduction of a factor 1.5 (∼15) is expected for KamLAND-Zen 800 (KamLAND2-Zen).

nEXO [87] is an upgrade of the EXO-200 [55] experiment. The detector is a liquid time projection chamber (TPC) filled with 5 tons of xenon enriched at 90% in ^{136}Xe. One of the main background contributions expected in nEXO is due to radioactive isotopes in the TPC materials. Because of the self-shielding of the Xe material, the rate of background events decreases exponentially moving toward the center. The collaboration plans to perform an analysis of the full detector volume, using the outer part to constrain the external background contribution. Our counting analysis cannot accommodate this directly and we are forced to tune the sensitive background and exposure. Given a fiducial volume of 3 tons of Xe, a ROI of (Q value $\pm 1.2\sigma$) and an average background level of $\sim 4 \times 10^{-6}$ cts/keV/kg$_{\rm iso}$/yr (that is ∼20% of the reference value [64,88]), we obtain a discovery sensitivity 15%–20% lower than the collaboration's

estimate. This is however sufficient for our analysis. The instrumental efficiency is taken for EXO-200 [55]. In nEXO, the energy resolution is expected to be improved by a factor of 1.2, and the background level reduced by about a factor of 400 with respect to EXO-200, due primarily to better self-shielding and more efficient background identification in the larger experiment.

NEXT [65] aims to search for $0\nu\beta\beta$ decay using a high-pressure Xe-gas TPC, which combines tracking capabilities with a low background typical of experiments with a single element in the active volume. The expected presence of the ^{214}Bi gamma line at 2447 keV in the vicinity of the $0\nu\beta\beta$ decay Q value at 2458 keV requires the use of an asymmetric ROI [75]. A single TPC with 100 kg of Xe (90% ^{136}Xe) and a resolution of 0.75% FWHM [75] will be used in the next phase of the project (NEXT 100). In a later stage, the collaboration plans to operate an array of three TPCs, each with a total Xe mass of 500 kg, a background level lower by a factor ∼10 with respect to NEXT 100, and an improved energy resolution of 0.5% FWHM [76] (NEXT 1.5k) [76]. The total efficiency is taken from [75]: the value reported in Table I does not contain the fiducial volume fraction (88%) and the fraction of events in the ROI (90%). We compared the NEXT 100 exclusion sensitivity obtained with our approach with that given in [75], and find that the two values agree within ∼10%.

Another experiment using the same technique as NEXT is PandaX. After two phases dedicated to dark matter searches, a $0\nu\beta\beta$ decay search program—denoted PandaX-III—is planned [66]. The TPC of PandaX-III will be about twice as big as that of NEXT, but will have an energy resolution of about 3% FWHM [66]. As for NEXT, one of the major expected backgrounds is ^{214}Bi. Consequently, an asymmetric ROI would yield a higher sensitivity, but for consistency with Ref. [66] we used a ROI of (Q value $\pm 2\sigma$). We could not find information regarding the size of the fiducial volume, and we assume it to be 100%. The total efficiency is about 35% [66]. In a second stage, the PandaX-III collaboration plans to construct four additional TPCs with energy resolution improved to 1% FWHM and a background level reduced by 1 order of magnitude. Our evaluation of the exclusion sensitivity agrees at the ∼10% level with the official value [66].

[1] T. Kajita, Rev. Mod. Phys. **88**, 030501 (2016).
[2] A. B. McDonald, Rev. Mod. Phys. **88**, 030502 (2016).
[3] K. Eguchi *et al.* (KamLAND Collaboration), Phys. Rev. Lett. **90**, 021802 (2003).
[4] C. Patrignani *et al.* (Particle Data Group Collaboration), Chin. Phys. C **40**, 100001 (2016).
[5] E. Majorana and L. Maiani, Il Nuovo Cimento **14**, 171 (1937).
[6] J. D. Vergados, H. Ejiri, and F. Simkovic, Rep. Prog. Phys. **75**, 106301 (2012).
[7] M. Fukugita and T. Yanagida, Phys. Lett. B **174**, 45 (1986).
[8] B. Kayser, Phys. Scr. **2005**, 156.
[9] W. H. Furry, Phys. Rev. **56**, 1184 (1939).
[10] J. Schechter and J. W. F. Valle, Phys. Rev. D **25**, 2951 (1982).
[11] M. Duerr, M. Lindner, and A. Merle, J. High Energy Phys. 06 (2011) 091.
[12] I. Esteban, M. C. Gonzalez-Garcia, M. Maltoni, I. Martinez-Soler, and T. Schwetz, J. High Energy Phys. 01 (2017) 087.
[13] P. Adamson *et al.* (NOvA Collaboration), Phys. Rev. Lett. **118**, 231801 (2017).
[14] K. Abe *et al.* (T2K Collaboration), Phys. Rev. Lett. **118**, 151801 (2017).
[15] M. Blennow, P. Coloma, P. Huber, and T. Schwetz, J. High Energy Phys. 03 (2014) 028.
[16] F. Capozzi, E. Di Valentino, E. Lisi, A. Marrone, A. Melchiorri, and A. Palazzo, Phys. Rev. D **95**, 096014 (2017).
[17] W. Rodejohann, Int. J. Mod. Phys. E **E20**, 1833 (2011).
[18] J. Zhang and S. Zhou, Phys. Rev. D **93**, 016008 (2016).
[19] F. F. Deppisch, P. S. Bhupal Dev, and A. Pilaftsis, New J. Phys. **17**, 075019 (2015).
[20] T. Peng, M. J. Ramsey-Musolf, and P. Winslow, Phys. Rev. D **93**, 093002 (2016).
[21] P. A. R. Ade *et al.* (Planck Collaboration), Astron. Astrophys. **594**, A13 (2016).
[22] S. Dell'Oro, S. Marcocci, M. Viel, and F. Vissani, J. Cosmol. Astropart. Phys. 12 (2015) 023.
[23] E. Fermi, Z. Phys. **88**, 161 (1934).
[24] E. Fermi, Nuovo Cimento **11**, 1 (1934).
[25] V. N. Aseev *et al.* (Troitsk Collaboration), Phys. Rev. D **84**, 112003 (2011).
[26] C. Kraus *et al.*, Eur. Phys. J. C **40**, 447 (2005).
[27] A. Gando *et al.* (KamLAND-Zen Collaboration), Phys. Rev. Lett. **117**, 082503 (2016); A. Gando *et al.* (KamLAND-Zen Collaboration), Phys. Rev. Lett. **117**, 109903 (2016).
[28] M. Agostini *et al.* (GERDA Collaboration), Nature (London) **544**, 47 (2017).
[29] J. Engel and J. Menéndez, Rep. Prog. Phys. **80**, 046301 (2017).
[30] F. Feruglio, A. Strumia, and F. Vissani, Nucl. Phys. **B637**, 345 (2002); F. Feruglio, A. Strumia, and F. Vissani, Nucl. Phys. **B659**, 359 (2003).
[31] S. F. King, A. Merle, and A. J. Stuart, J. High Energy Phys. 12 (2013) 005.
[32] M. Agostini, A. Merle, and K. Zuber, Eur. Phys. J. C **76**, 176 (2016).

[33] N. Nath, M. Ghosh, S. Goswami, and S. Gupta, J. High Energy Phys. 03 (2017) 075.
[34] S. Davidson, G. Isidori, and A. Strumia, Phys. Lett. B **646**, 100 (2007).
[35] G. Cowan, K. Cranmer, E. Gross and O. Vitells, arXiv: 1105.3166.
[36] F. Šimkovic, V. Rodin, A. Faessler, and P. Vogel, Phys. Rev. C **87**, 045501 (2013).
[37] J. Hyvärinen and J. Suhonen, Phys. Rev. C **91**, 024613 (2015).
[38] M. T. Mustonen and J. Engel, Phys. Rev. C **87**, 064302 (2013).
[39] J. Menéndez, A. Poves, E. Caurier, and F. Nowacki, Nucl. Phys. **A818**, 139 (2009).
[40] M. Horoi and A. Neacsu, Phys. Rev. C **93**, 024308 (2016).
[41] J. Barea, J. Kotila, and F. Iachello, Phys. Rev. C **91**, 034304 (2015).
[42] N. López Vaquero, T. R. Rodríguez, and J. L. Egido, Phys. Rev. Lett. **111**, 142501 (2013).
[43] J. M. Yao, L. S. Song, K. Hagino, P. Ring, and J. Meng, Phys. Rev. C **91**, 024316 (2015).
[44] A. Caldwell, D. Kollar, and K. Kröninger, Comput. Phys. Commun. **180**, 2197 (2009).
[45] G. Benato, Eur. Phys. J. C **75**, 563 (2015).
[46] M. Gerbino, M. Lattanzi, and A. Melchiorri, Phys. Rev. D **93**, 033001 (2016).
[47] M. Gerbino, M. Lattanzi, O. Mena, and K. Freese, arXiv: 1611.07847.
[48] N. Palanque-Delabrouille *et al.*, J. Cosmol. Astropart. Phys. 02 (2015) 045.
[49] O. Cremonesi and M. Pavan, Adv. High Energy Phys. **2014**, 951432 (2014).
[50] S. Dell'Oro, S. Marcocci, M. Viel and F. Vissani, Adv. High Energy Phys. **2016**, 2162659 (2016).
[51] K. H. Ackermann *et al.* (GERDA Collaboration), Eur. Phys. J. C **73**, 2330 (2013).
[52] N. Abgrall *et al.* (Majorana Collaboration), Adv. High Energy Phys. **2014**, 365432 (2014).
[53] C. Arnaboldi *et al.* (CUORE Collaboration), Nucl. Instrum. Methods Phys. Res., Sect. A **518**, 775 (2004).
[54] D. R. Artusa *et al.* (CUORE Collaboration), Adv. High Energy Phys. **2015**, 879871 (2015).
[55] J. B. Albert *et al.* (EXO-200 Collaboration), Nature (London) **510**, 229 (2014).
[56] P. Ferrario, http://next.ific.uv.es/DocDB/0003/000359/001/Cambridge2017_web.pdf, 2017.
[57] R. Arnold *et al.*, Nucl. Instrum. Methods Phys. Res., Sect. A **536**, 79 (2005).
[58] NSAC NLDBD Subcommittee, Report to the nuclear science advisory committee: Neutrinoless double-beta decay, 2015, http://science.energy.gov/np/nsac/reports.
[59] G. Wang *et al.* (CUPID Collaboration), arXiv:1504.03599.
[60] G. Wang *et al.* (CUPID Collaboration), arXiv:1504.03612.
[61] J. Shirai, 2016, http://neutrino2016.iopconfs.org/IOP/media/uploaded/EVIOP/event_948/09.45__5__Shirai.pdf.
[62] B. Schwingenheuer, in CERN EP Seminar, Geneva, Switzerland, 2017, https://indico.cern.ch/event/581028/attachments/1395349/2129744/ge76_cern.pdf.
[63] S. Schönert, in *NeuTel 2017, Venice, Italy* (2017), https://agenda.infn.it/getFile.py/access?contribId=27&sessionId=9&resId=0&materialId=slides&confId=11857.
[64] B. Mong (nEXO Collaboration), Proc. Sci., HQL2016 (**2017**) 074.
[65] V. Alvarez *et al.* (NEXT Collaboration), J. Instrum. **7**, T06001 (2012).
[66] X. Chen *et al.*, Sci. China Phys. Mech. Astron. **60**, 061011 (2017).
[67] V. Lozza (SNO+ Collaboration), in *Proceedings, Magellan Workshop, Hamburg, Germany, 2016* (Magellan Workshop, Hamburg, Germany, 2016), pp. 87–94, http://bib-pubdb1.desy.de/record/315080.
[68] J. Klein (SNO+ Collaboration), http://www.physics.upenn.edu/~jrk/talks/nsac_nldbd.pdf.
[69] P. P. Povinec (SuperNEMO Collaboration), Nucl. Instrum. Methods Phys. Res., Sect. A **845**, 398 (2017).
[70] R. Arnold *et al.* (SuperNEMO Collaboration), Eur. Phys. J. C **70**, 927 (2010).
[71] G. Cowan, K. Cranmer, E. Gross, and O. Vitells, Eur. Phys. J. C **71**, 1554 (2011); G. Cowan, K. Cranmer, E. Gross, and O. Vitells, Eur. Phys. J. C **73**, 2501(E) (2013).
[72] D. R. Artusa *et al.* (CUORE Collaboration), Eur. Phys. J. C **74**, 3096 (2014).
[73] K. Singh, http://www.rcnp.osaka-u.ac.jp/dbd16/Data/Prog/041_SNO+_KalpanaSingh.pdf, 2016.
[74] B. Mong, 2016, http://indico.phys.vt.edu/event/31/session/29/contribution/103/material/slides/0.pdf.
[75] J. Martín-Albo *et al.* (NEXT Collaboration), J. High Energy Phys. 05 (2016) 159.
[76] J. J. Gomez-Cadenas, in XLV International Meeting on Fundamental Physics, Granada, Spain [https://indico.cern.ch/event/589204/contributions/2413789/attachments/1453832/2242882/GranadaDBM.pdf, 2017].
[77] J. Angrik *et al.* (KATRIN Collaboration), KATRIN Design Report No. 7090, 2004, https://www.katrin.kit.edu/publikationen/DesignReport2004-12Jan2005.pdf.
[78] S. Mertens, J. Phys. Conf. Ser. **718**, 022013 (2016).
[79] F. Simpson, R. Jimenez, C. Pena-Garay, and L. Verde, J. Cosmol. Astropart. Phys. 06 (2017) 029.
[80] A. Caldwell, A. Merle, O. Schulz, and M. Totzauer, arXiv: 1705.01945.
[81] G. Punzi, Proceedings of the Conference on Statistical Problems in Particle Physics, Astrophysics and Cosmology, https://www.slac.stanford.edu/econf/C030908/papers/SLAC-R-703.pdf.
[82] C. Alduino *et al.* (CUORE Collaboration), Phys. Rev. C **93**, 045503 (2016).
[83] C. Alduino *et al.* (CUORE Collaboration), arXiv:1704.08970.
[84] F. Alessandria *et al.*, arXiv:1109.0494.
[85] M. Chen, J. Klein, and G. Orebi Gann (private communication).
[86] A. Gando *et al.* (KamLAND-Zen Collaboration), Phys. Rev. Lett. **110**, 062502 (2013).
[87] A. Pocar (nEXO, EXO-200 Collaboration), Proc. Sci., NEUTEL2015 (**2015**) 049.
[88] L. Yang, 2016, https://neutrino2016.iopconfs.org/IOP/media/uploaded/EVIOP/event_948/10.05__5__ Yang.pdf.